SPECT IMAGE RECONSTRUNTION USING COMPOUND PRIOR MODELS

Antonio López[1]*, Rafael Molina[2], Aggelos K. Katsaggelos[3], and Javier Mateos[2]

[1] *Departamento de Lenguajes y Sistemas Informáticos, Universidad de Granada. 18071 Granada, Spain. alopez@ugr.es*

[2] *Departamento de Ciencias de la Computación e I. A., Universidad de Granada. 18071 Granada, Spain. {rms,jmd}@decsai.ugr.es*

[3] *Department of Electrical and Computer Engineering, Northwestern University. Evaston, Illinois 60208-3118. aggk@ece.nwu.edu*

Abstract

We propose a new iterative method for Maximum a Posteriori (MAP) reconstruction of SPECT (Single Photon Emission Computed Tomography) images. The method uses Compound Gauss Markov Random Fields (CGMRF) as prior model and is stochastic for the line process and deterministic for the reconstruction. Synthetic and real images are used to compare the new method with existing ones.

Keywords: SPECT imaging; compound Gauss Markov random fields; Bayesian reconstruction; simulated annealing; deterministic image reconstruction.

1 Introduction

SPECT images are observation data acquired by a gamma-camera following an orbit around the patient's body, at regularly spaced angles. A reconstructed image is the discrete representation of a slice or cross section of the isotope distribution within the patient, transversal to the gamma-camera rotation axis.

Bayesian reconstruction methods have been extensively used to reconstruct medical images since they can improve the reconstructions with respect to the classical non statistical methods, such as FBP (Filtered Back Projection)[15] and ART (Algebraic Reconstruction Techniques).[25]

In the Bayesian paradigm, the reconstructed image $\hat{X}$ is usually selected as

$$\hat{X} = \arg\max_X P(X|Y) = \arg\max_X P(Y|X)P(X), \quad (1)$$

*Author for correspondence

where $P(X)$ is a prior distribution incorporating information about the expected structure in the image X, and $P(Y|X)$ models the degradation process of projections Y from the pixel intensities of the emission source (patient).

When the energy function associated with the prior distribution is convex, pure descent algorithms assure that the global minimum of $-\ln P(X|Y)$ can be found.[3] However, when the prior model explicitly favors the presence of discontinuities, the energy of the posterior distribution of the reconstruction given the data usually presents many local minima. In this case stochastic algorithms such as simulated annealing, [11,23] deterministic methods[2,6,5] and mixed-annealing algorithms,[22,1] where stochastic steps alternate with deterministic ones, have been proposed. Unfortunately all these methods assume that the degradation process is Gaussian.

For SPECT images, a problem where the degradation process is Poisson, several reconstruction methods have been proposed that fit within the Bayesian framework (see, for instance [29,30,12,3,13,10,21,27,17,16]). General strategies to find the MAP have been proposed. [9,8,4,7] However, no much work has been reported on the use of Compound Gauss Markov Random Fields (CGMRF) to reconstruct such images (see however [18,24,19]).

In this work we propose a Bayesian technique for SPECT image reconstruction that uses Compound Gauss Markov Random Fields (CGMRF) as prior model and is stochastic for the line process and deterministic for the image process when computing their respective MAP estimates.

The rest of the paper is organized as follows. In section 2 we define the observation and image models. Then, in section 3 we propose a new method for finding the MAP estimate. The application of this method to synthetic and real images is described in section 4. Finally, section 5 concludes the paper.

2 Observation and image models

The observation model for emission tomography can be specified as a product of independent Poisson distributions[29]

$$P(Y|X) = \prod_{s=1}^{M} \frac{(\sum_{i=1}^{N} A_{s,i}x_i)^{y_s} \exp\{-\sum_{t=1}^{N} A_{s,t}x_t\}}{y_s!}, \tag{2}$$

where M is the number of detectors, N is the number of pixels and A is the system matrix, $A_{s,i}$ is the probability that an emitted photon from pixel i reaches detector s.

The prior model we use is a CGMRF model. This model provides us with a means to control changes in the image using a hidden random field. A CGMRF model has two levels, an upper level which is the image to be restored and the lower or hidden level, called the line process, which is an underlying random field governing the transition between sub-models. The use of a line process, was introduced by Geman and Geman[11] for the discrete case. Extensions to the continuous case were presented by Jengs and Woods[14] (see also [18] for medical image reconstruction).

The CGMRF model to be used here is introduced from a simpler one, the Conditional Auto-Regression (CAR) model.[26] This prior model is defined by

$$P(X) \propto \exp\left\{-\frac{1}{2}\alpha\, X^t(I-\phi C)X\right\} \tag{3}$$

where α is a scaling parameter, for an 8-point neighborhood system, the (i,j)th element of matrix C is given by

$$C_{i,j} = \begin{cases} 2(0.5\sqrt{2}+1)^{-1} & \text{if } d(i,j)=1 \\ 2(\sqrt{2}+1)^{-1} & \text{if } d(i,j)=\sqrt{2} \\ 0 & \text{otherwise} \end{cases}$$

$d(i,j)$ is the Euclidean distance between pixels i and j (see [28]) and $|\phi| < 1/8$. Note that $\sum_j C_{i,j} = 8$ and since (see [26])

$$E\left[x_i | x_j,\, j \neq i\right] = \phi \sum_j C_{i,j} x_j, \tag{4}$$

when ϕ is just less than $1/8$, Eq. (4) means that the expectation of a pixel x_i given the rest of the image is similar to the mean of its eight neighbors weighted according to their distance to the pixel x_i.

INSERT FIGURE 1 HERE

If we assume a "toroidal edge correction", we introduce the line process by rewriting Eq. (3) as

$$\begin{aligned} -\log P(X,L) \propto & \\ & \frac{\alpha\phi}{2}\left(\sum_i C_{i,i:1}(x_i - x_{i:1})^2(1-l_{[i,i:1]}) + \sum_i C_{i,i:2}(x_i - x_{i:2})^2(1-l_{[i,i:2]})\right) + \\ & \frac{\alpha\phi}{2}\left(\sum_i C_{i,i:5}(x_i - x_{i:5})^2(1-l_{[i,i:5]}) + \sum_i C_{i,i:6}(x_i - x_{i:6})^2(1-l_{[i,i:6]})\right) + \\ & \frac{\alpha}{2}\sum_i \beta\left[l_{[i,i:1]} + l_{[i,i:2]} + l_{[i,i:5]} + l_{[i,i:6]}\right] + \frac{\alpha}{2}\sum_i (1-8\,\phi)x_i^2, \end{aligned} \tag{5}$$

where $i{:}1,\ i{:}2, ...,\ i{:}8$ are the eight pixels around pixel i (see figure 1). If all the elements $l([i,j])$ take always the value zero we have a CAR model. However, if $l([i,j])$ takes the value zero if pixels i and j are not separated by an active line and one otherwise we have a CGMRF model. The parameter β is a scalar weight, which adjusts the introduction of the active line elements. For β very large the prior model becomes Gaussian. The line process acts as inhibitor or activator of the relation between two neighboring pixels depending on whether or not there exists an edge.

3 MAP estimation

Let us now proceed to find $\hat{X}$, $\hat{L}$, the MAP estimates of X and L, that is

$$\hat{X}, \hat{L} = \arg\max_{X,L} P(X, L|Y). \tag{6}$$

The method we propose for estimating the original image and the line process is stochastic for the line process and deterministic for the reconstruction, as we will describe now.

In order to estimate the line process we simulate the corresponding conditional *a posteriori* density function. Let us denote by $P_T(l_{[i,j]}|L_{[i,j]}, X, Y)$ the conditional *a posteriori* density function for the line process element $l_{[i,j]}$, given X, Y and the rest of L, $(L_{[i,j]} = (l_{[s,t]} : \forall [s,t] \neq [i,j]))$. To simulate this density function, we have

$$P_T(l_{[i,j]} = 0|L_{[i,j]}, X, Y) \propto \exp\left[-\frac{1}{T}\frac{\alpha\phi C_{i,j}}{2}(x_i - x_j)^2\right] \tag{7}$$

$$P_T(l_{[i,j]} = 1|L_{[i,j]}, X, Y) \propto \exp\left[-\frac{1}{T}\frac{\alpha\beta}{2}\right], \tag{8}$$

where T is the temperature.

Given an estimate of the line process, L, and the observation, Y, we note that $-\ln P(X|L,Y)$ is convex in X and so a simple gradient method can be used to minimize it. A different more efficient procedure is followed in estimation the image X, as described next. Starting from the probability distribution $P(X|L,Y)$ we have

$$\begin{aligned} -\frac{\partial}{\partial x_i}\ln P(X|L,Y) &= 1 - \sum_{s=1}^{M}\frac{y_s A_{s,i}}{\sum_{t=1}^{N} A_{s,t}x_t} \\ &+ \alpha\phi\sum_{j\in\mathcal{N}_i} C_{i,j}(x_i - x_j)(1 - l_{[i,j]}) + \alpha(1 - 8\,\phi)x_i \end{aligned}$$

and so at the minimum of $-\ln P(X|L,Y)$ we have

$$\begin{aligned} 1 + \alpha x_i \left\{\phi\sum_{j\in\mathcal{N}_i} C_{i,j}(1 - l_{[i,j]}) + (1 - 8\phi)\right\} \\ = \sum_{s=1}^{M}\frac{y_s A_{s,i}}{\sum_{t=1}^{N} A_{s,t}x_t} + \alpha\phi\sum_{j\in\mathcal{N}_i} C_{i,j}x_j(1 - l_{[i,j]}) \end{aligned}$$

Now, taking into account that $\phi\sum_{j\in\mathcal{N}_i} C_{i,j} + (1 - 8\,\phi) = 1$ and noting that when $l_{[i,j]} = 1$, $x_i(1 - l_{[i,j]}) = 0$ and $x_j(1 - l_{[i,j]}) = 0$, at the minimum of $-\ln P(X|L,Y)$ we have

$$1 + \alpha x_i = \sum_{s=1}^{M}\frac{y_s A_{s,i}}{\sum_{t=1}^{N} A_{s,t}x_t} + \alpha\phi\sum_{j\in\overline{\mathcal{N}}_i} x_j C_{i,j} + \alpha\phi x_i\sum_{j\in\underline{\mathcal{N}}_i} C_{i,j} \tag{9}$$

where $\overline{\mathcal{N}}_i$ and $\underline{\mathcal{N}}_i$ denote, respectively, the neighboring pixels of i without or with an active line between i and j. We have removed their dependency on the current line process estimate for simplicity.

Then, multiplying both sides of Eq. (9) by $x_i/(1+\alpha x_i)$ we obtain that the image X maximizing $P(X|L,Y)$ satisfies for all i

$$x_i = \mu_i \left(\phi \sum_{j \in \overline{\mathcal{N}}_i} x_j C_{i,j} + \phi x_i \sum_{j \in \underline{\mathcal{N}}_i} C_{i,j} \right) + (1-\mu_i) x_i \sum_{s=1}^{M} \frac{y_s A_{s,i}}{\sum_{t=1}^{N} A_{s,t} x_t}, \quad (10)$$

with $\mu_i = \alpha x_i/(\alpha x_i + 1)$.

This equation is used to define an iterative process. Using the current estimate of the original image in the right hand side of Eq. (10) we obtain a new estimate of it.

Furthermore the proposed iterative method is a modification of Newton's method[20] since from Eq. (10) we have

$$x_i^{new} = x_i^{old} + \frac{x_i^{old}}{1+\alpha x_i^{old}} \frac{\partial}{\partial x_i} \ln P(X|L,Y) \quad (11)$$

and so it can be written as

$$X^k = X^{k-1} - M^{k-1} \nabla [-\ln P(X^{k-1}|L,Y)]^t \quad (12)$$

where k denotes iteration and M^{k-1} is a diagonal matrix with entries $1/(1+\alpha x_i^{k-1})$. We have used this iterative scheme in our test examples and observed experimentally that it converges. We also note that the proposed method does not need to calculate either the Hessian matrix or the optimal step of the gradient. Furthermore, if we start the iteration with a nonegative image estimate, the iterative process in Eq. (10) is guaranteed to provide always non negative images and that when $\alpha = 0$ we obtain the classical E-M algorithm for Poisson distributions.

Let us now summarize and describe how to use Eqs. (7), (8) and (10) to find the MAP estimate of L and X:

Let $k = 1, 2, ...$, be the sequence of iterations in which the sites (lines or pixels) are visited for updating.

1. Set $k = 0$ and assign an initial configuration, X^{-1}, L^{-1}, and an initial temperature $T = 1$.

2. The evolution $\hat{L}^{k-1} \rightarrow \hat{L}^k$ of the whole line process is simulated by the probability functions defined in Eqs. (7) and (8).

3. The evolution $\hat{X}^{k-1} \rightarrow \hat{X}^k$ of the whole image is obtained using $\hat{X}^{k-1}$ in the right hand side of Eq. (10) to obtain $\hat{X}^k$ in the left hand side of the same equation.

4. Set $k = k + 1$. Decrease the temperature T according to an annealing scheme.[14] Go to step 2 until to fit a stopping criterion.

4 Experimental results

Let us examine how the proposed method works on both synthetic and real images.

INSERT FIGURE 2 HERE

Figure 2 shows the results for the 128×128 synthetic image depicted in Fig. 2(a). The sinogram, shown in Fig. 2(b), was simulated assuming a system with 128 detectors equipped with a parallel hole collimator that described a semicircular orbit with 128 angles. The simulation assumed Poisson noise and no attenuation during the capturing process.

Figure 2(e) shows the reconstruction of this sinogram with the proposed method. The used parameters were chosen experimentally to be $\alpha = 19^{-1}$ and $\beta = 15.4$. The stopping criterion was $||X^k - X^{k-1}||^2/||X^k||^2 < 10^{-9}$. The corresponding line process (Fig. 2(f)) shows that the method locates all the regions in the image and the general form of the objects is clearly distinguished.

In order to compare the results, other reconstruction methods using a Conditional Autoregressive (CAR) prior and a Generalized Gauss-Markov Random Field (GGMRF)[3] prior were applied to the sinogram in Fig. 2(b). The parameters needed for these reconstruction methods were $\alpha = 280^{-1}$ for the CAR prior and, for the GGMRF, $\sigma^{1.1} = 18$ for a shape parameter $p = 1.1$. Results are shown in Fig. 2(c) for the CAR prior and Fig. 2(d) for the GGMRF prior.

We can observe that the CAR prior penalizes in excess the edges while both the GGMRF and the proposed CGMRF priors better preserve them. It is important to note that the shape parameter in the GGMRF prior plays an important role in the edge preservation obtaining better results when it is close to 1. We fixed it to 1.1 since, experimentally, we observed that best results were obtained in that case. The CGMRF model provides much sharper edges and zones inside the regions are more uniform and similar to the original image.

We note that the CAR prior is a special case of both the GGMRF and CGMRF priors. The GGMRF prior generates the CAR prior when the shape parameter is set equal to 2 and, as noted previously, the CGMRF is equivalent to the CAR prior when β is very large. Note, however, that, in the presence of edges, the variance of the prior distribution, the inverse of the parameter α, is greater for the CAR prior than for the CGMRF one. Since the CAR prior does not take into account the presence of edges, the variance of the model increases due to the difference between the pixel in both sides of an edge. However, the CGMRF prior takes into account that pixels across the edges are not related and, hence, the variance of the model, and so the variance within regions, decreases.

INSERT FIGURE 3 HERE

Another example with a synthetic image is shown in Fig. 3. The simulation process from the original image (Fig. 3(a)) to the corresponding sinogram (Fig. 3(b)) was performed as in the previous example. Reconstruction with the proposed method with $\alpha = 24.5^{-1}$ and $\beta = 17.5$ is shown in Fig. 3(e) and, its

corresponding line process, in Fig. 3(f). Results for the CAR prior ($\alpha = 563$) and the GGMRF prior ($\sigma^{1.1} = 21.2$ for a shape parameter $p = 1.1$), are depicted in Fig. 3(c) and Fig. 3(d), respectively. As in the previous test, the CAR prior oversmooths the edges, furthermore, it produces artifacts in the interior areas. Sharper edges and smooth areas are obtained for the CGMRF prior which, also, recognized all the regions quite accurately.

INSERT FIGURE 4 HERE

The method was also tested on real data obtained by a Siemens Orbiter 66601 detector with the collimator being a parallel hole. The gamma-camera, equipped with 64 detectors, described a circular orbit, at 5.625 degrees steps (64 angles). Therefore, the size of the real image is 64×64. The data corresponds to the inferior part of the liver (the right lobe and the center posterior hepatic zone, crossed there by blood vessels). The data provided by the detector system and its FBP reconstruction are shown in Fig. 4(a) and (b), respectively. Looking at the figure it is clear that the CAR, GGMRF and CGMRF prior methods (depicted in Fig. 4(c), (d) and (e), respectively) provide better results than FBP (see Fig. 4(c)) although, the CAR prior oversmooths the edges. The CGMRF prior method again provides better results than the CAR and the GGMRF ones since areas with different levels of vascularization can be better distinguished. More concretely, the vessel in the center part of the image, barely distinguished in the GGMRF reconstruction is clear and sharp in the CGMRF one. Also, the shade around the central objects, due to the refraction on other organs near to the liver, is better eliminated by this method.

INSERT FIGURE 5 HERE

INSERT FIGURE 6 HERE

In order to test the convergence of the method we run our method on different fixed line process configurations (see Fig. 6). We obtained in all our tests, a continuous increment in the log-likelihood (see Fig. 5(a)) and, also, a continuous decrease of the norm of the difference between two consecutive iterations (Fig. 5(b)).

5 Conclusions

In this paper we have presented a new method that can be used to reconstruct SPECT images. This method uses a prior model with a line process and the MAP estimation is performed by simulated annealing for the line process and a deterministic iterative scheme for the image. This iterative scheme has been shown to converge experimentally and to provide always non negative solutions when the iteration starts with a nonegative image. The experimental results demonstrate the improved performance of the proposed algorithm over other competing algorithms.

Acknowledgment

This work has been partially supported by the "CICYT" (Comisión Nacional de Ciencia y Tecnología) under contract TIC2000-1275.

References

1. L. Bedini, M. del Corso and A. Tonazzini, "A precondtioning technique for edge preserving image restoration," in *Proceedings of the Int. Conf. on Information Intelligence and Systems, ISNLS-99*, 1999, pp. 519-526.

2. A. Blake and A. Zisserman, *Visual Reconstruction*, MIT Press, 1987.

3. C. Bouman and K. Sauer, "A generalized Gaussian image model for edge-preserving MAP estimation," *IEEE Trans. Image Processing* **2**, 3 (1993) 296-310.

4. C. L. Byrne, "Iterative image reconstruction algorithms based on cross-entropy minimization," *IEEE Trans. Image Processing* **2**, 1 (1993) 96-103.

5. R. H. Chan and M. K. Ng, "Conjugate gradient method for toeplitz systems," *SIAM Review* **38** (1996) 427-482.

6. P. Charbonnier, L. Blanc-Féraud, G. Aubert and M. Barlaud, "Deterministic edge-preserving regularization in computed imaging," *IEEE Trans. on Image Processing* **6**, 12 (1997) 298-311.

7. A. DePierro, "A modified expectation maximization algorithm for penalized likelihood estimation in emission tomography," *IEEE Trans. Medical Imaging* **14**, 1 (1995) 132-137.

8. J. A. Fessler and S. D. Booth, "Conjugate-gradient preconditioning methods for shift-variant PET image reconstruction," *IEEE Trans. on Image Processing* **8**, 5 (1999) 688-699.

9. J. A. Fessler and A. O. Hero, "Penalized maximum-likelihood image reconstruction using space-alternating generalized EM algorithms," *IEEE Trans. on Image Processing* **4**, 10 (1995) 1417-1429.

10. D. Geman and C. Yang, "Nonlinear image recovery with half-quadratic regularization," *IEEE Trans. on Image Analysis* **4**, 7 (1995) 932-946.

11. S. Geman and D. Geman, "Stochastic relaxation, Gibbs distributions, and the Bayesian restoration of images," *IEEE Trans. Pattern Analysis and Machine Intelligence* **6**, 6 (1984) 721-741.

12. P. J. Green, "Bayesian reconstructions from emission tomography data using a modified EM algorithm," *IEEE Trans. on Medical Imaging* **9**, 1 (1990) 84-93.

13. T. J. Hebert and R. Leahy, "Statistic-based MAP image reconstruction from Poisson data using Gibbs priors," *IEEE Trans. on Signal Processing* **40**, 9 (1992) 2290-2303.

14. F. C. Jeng and J. W. Woods, "Simulated annealing in compound Gaussian random fields," *IEEE Trans. Information Theory* **36**, 1 (1990) 94-107.

15. A. C. Kak and M. Slaney, *Principles of Computerized Tomographic Imaging*, IEEE Press, 1988.

16. R. Leahy, "Recent developments in iterative image reconstruction for PET and SPECT," *IEEE Trans. Medical Imaging* **19**, 4 (2000) 257-259.

17. R. Leahy and X. Yan, "Incorporation of anatomical MR data for improved functional imaging with PET," in *Information Processing in Medical Imaging*, eds. A. C. Colchester and D. Hawkes, Springer Verlag, 1991 pp. 105-120.

18. S. Lee, A. Rangarajan and G. Gindi, "Bayesian image reconstruction in SPECT using high-order mechanical models as priors," *IEEE Trans. Medical Imaging* **14**, 4 (1995) 669-680.

19. A. López, R. Molina, A. K. Katsaggelos and J. Mateos, "SPECT image reconstruction using compound models," in *Proceedings of the Int. Conf. on Acoustics, Speech and Signal Processing, ICASSP-01*, volume 3, 2001, pp. 1909-1912.

20. D. Luenberger, *Linear and Nonlinear Programming*, Addison-Wesley, 1989.

21. P. Malick, P. Charbonnier, L. Blanc-Féraud, I. Laurette, J. Darcourt and M. Barlaud, "Poisson statistic and half-quadratic regularization for emission tomography reconstruction algorithms," in *Proceedings of the Int. Conf. on Image Processing, ICIP-96*, volume 2, 1996, pp. 729-732.

22. J. Marroquin, "Probabilistic solution of inverse problems," *MIT-AI 860, Artificial Intelligence Laboratory* (1985) MIT, cambridge, MA.

23. R. Molina, A. K. Katsaggelos, J. Mateos, A. Hermoso and A. Segall, "Restoration of severely blurred high range images using stochastic and deterministic relaxation algorithms in compound Gauss Markov random fields," *Pattern Recognition* **33**, 4 (2000) 555-571.

24. R. Molina and A. López, "SPECT image reconstruction," in *Plenary Session, Irish Machine Vision and Image Processing Conference (IMVIP)*, http://www.qub.ac.uk/ubs/imvip2000, 2000 .

25. P. Oskoui-Fard and H. Stark, "Tomographic image reconstruction using the theory of convex projections," *IEEE Trans. Medical Imaging* **7**, 1 (1988) 45-58.

26. B. Ripley, *Spatial Statistic*, Wiley, New York, 1981.

27. S. Saquib, *Edge-Preserving Models and Efficient Algorithms for Ill-Posed Inverse Problems in Image Processing*, Ph.D. thesis, Purdue University, 1997.

28. S. Saquib, C. Bouman and K. Sauer, "ML parameter estimation for Markov random fields, with applications to Bayesian tomography," Technical Report TR-ECE 95-24, School fo Electrical and Computer Eng., Purdue University, 1995.

29. L. Shepp and Y. Vardi, "Maximum likelihood reconstruction for emission tomography," *IEEE Trans. Medical Imaging* **1**, 2 (1982) 113-122.

30. Y. Vardi, L. Shepp and L. Kaufman, "A statistical model for positron emission tomography (with discussion)," *Journal of the American Statistical Association* **80**, 389 (1985) 8-37.

Antonio López was born in Granada, Spain, in 1964. He received a B. S. degree in physics with specialization in elctronic. He is a Professor of computer graphics in the Department of Software Engineering at the University of Granada. His areas of interest include image restoration, computer graphics and fractals. He is a member of the Eurographics.

Rafael Molina was born in 1957. He received the degree in mathematics (statistics) in 1979 and the Ph.D. degree in optimal design in linear models in 1983. He became Professor of computer science and artificial intelligence at the University of Granada, Granada, Spain, in 2000, and is currently the Dean of the Computer Engineering Faculty. His areas of research interest are image restoration (applications to astronomy and medicine), parameter estimation, image and video compression, and blind deconvolution. Dr. Molina is a member of SPIE, Royal Statistical Society, and the Asociación Española de Reconocimento de Formas y Análisis de Imágenes (AERFAI).

Aggelos K. Katsaggelos received the Diploma degree in electrical and mechanical engineering from the Aristotelian University of Thessaloniki, Thessaloniki, Greece, in 1979 and the M.S. and Ph.D. degrees both in electrical engineering from the Georgia Institute of Technology, Atlanta, Georgia, in 1981 and 1985, respectively.

In 1985 he joined the Department of Electrical Engineering and Computer Science at Northwestern University, Evanston, IL, where he is currently professor, holding the Ameritech Chair of Information Technology. He is also the Director of the Motorola Center for Communications. During the 1986-1987 academic year he was an assistant professor at Polytechnic University, Department of Electrical Engineering and Computer Science, Brooklyn, NY. His current research interests include image and video recovery, video compression, motion estimation, boundary encoding, computational vision, and multimedia signal processing and communications. Dr. Katsaggelos is a Fellow of the IEEE, an Ameritech Fellow, a member of the Associate Staff, Department of Medicine, at Evanston Hospital, and a member of SPIE. He is a member of the Publication Boards of the IEEE Signal Processing Society and the *IEEE Proceedings*, the IEEE TAB Magazine Committee, the IEEE Technical Committees on Visual Signal Processing and Communications, and Multimedia Signal Processing, Editorial Board Member of Academic Press, Marcel Dekker: Signal Processing Series, *Applied Signal Processing*, and *Computer Journal*, and editor-in-chief of the *IEEE Signal Processing Magazine*. He has served as an Associate editor for the *IEEE Transcations on Signal Processing* (1990-1992), an area editor for the journal *Graphical Models and Image Processing* (1992-1995), a member of the Steering Committees of the *IEEE Transactions on Image Processing* (1992-1997) and the *IEEE Transactions on Medical Imaging* (1990-1999), a member of the IEEE Technical Committee on Image and Multi-Dimensional Signal Processing (1992-1998), and a member of the Board of Governors of the IEEE Signal Processing Society (1999-2001). He is the editor of *Digital Image Restoration* (Springer-Verlag, Heidelberg, 1991), co-author of *Rate-Distortion Based Video*

Compression (Kluwer Academic Publishers, 1997), and co-editor of *Recovery Techniques for Image and Video Compression and Transmission,* (Kluwer Academic Publishers, 1998). He has served as the General Chairman of the 1994 Visual Communications and Image Processing Conference (Chicago, IL), and as technical program co-chair of the 1998 IEEE International Conference on Image Processing (Chicago, IL). He is the the coinventor of eight international patents, and the recipient of the IEEE Third Millennium Medal (2000), the IEEE Signal Processing Society Meritorious Service Award (2001), and an IEEE Signal Processing Society Best Paper Award (2001).

Javier Mateos was born in Granada, Spain, in 1968. He received the Diploma and M. S. degrees in Computer Science from the University of Granada in 1990 and 1991, respectively, and completed his Ph. D. in Computer Science at the University of Granada in July 1998.

Since 1992, he has been Assistant Professor at the Department of Computer Science and Artificial Inteligence of the University of Granada and became Associate Professor in 2001. His research interests include image restoration and image and video recovery and compression. He is a member of the AERFAI (Asociación Española de Reconocimento de Formas y Análisis de Imágenes).

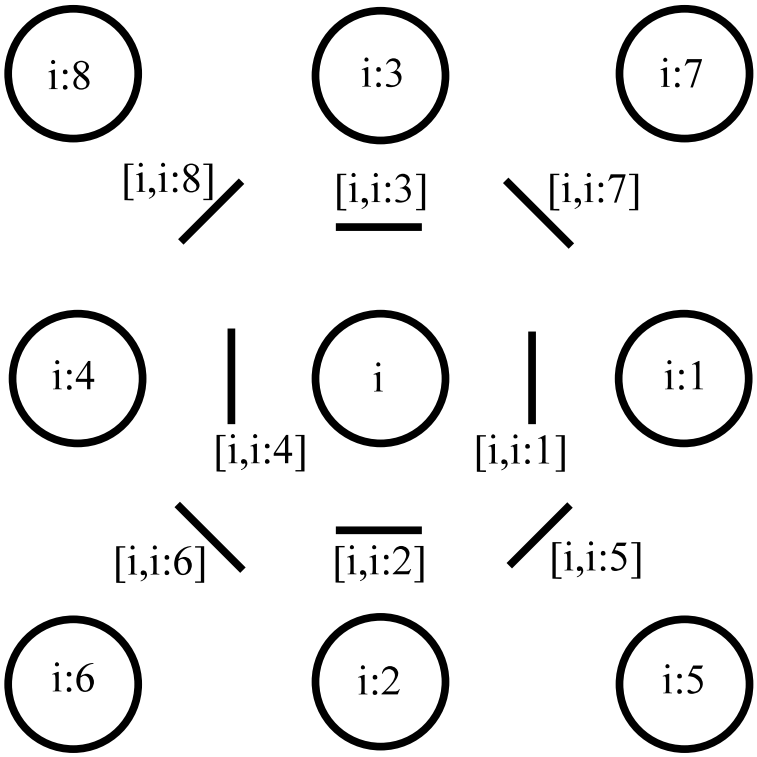

Figure 1: Image and line sites

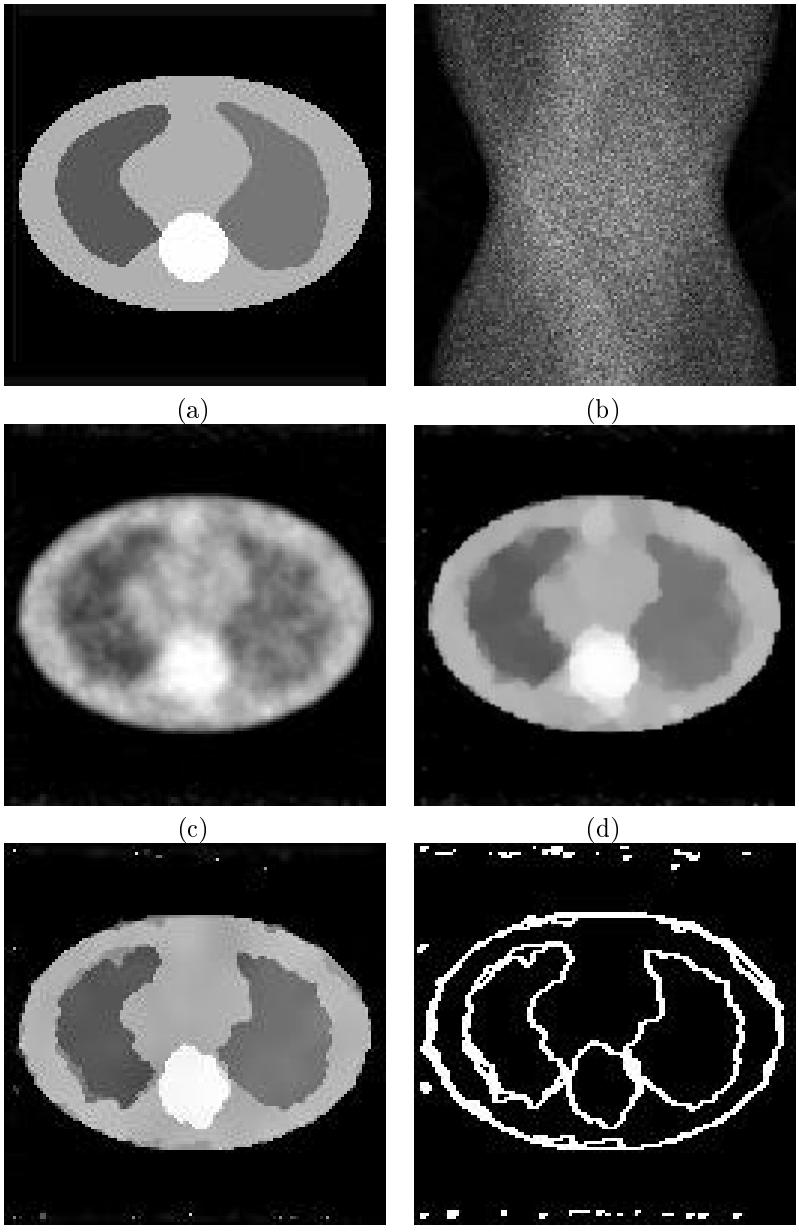

Figure 2: (a) Original image. (b) Simulated sinogram. Reconstruction using a (c) CAR prior, (d) GGMRF prior and (e) CGMRF prior. (f) Line process corresponding to the reconstruction in (e).

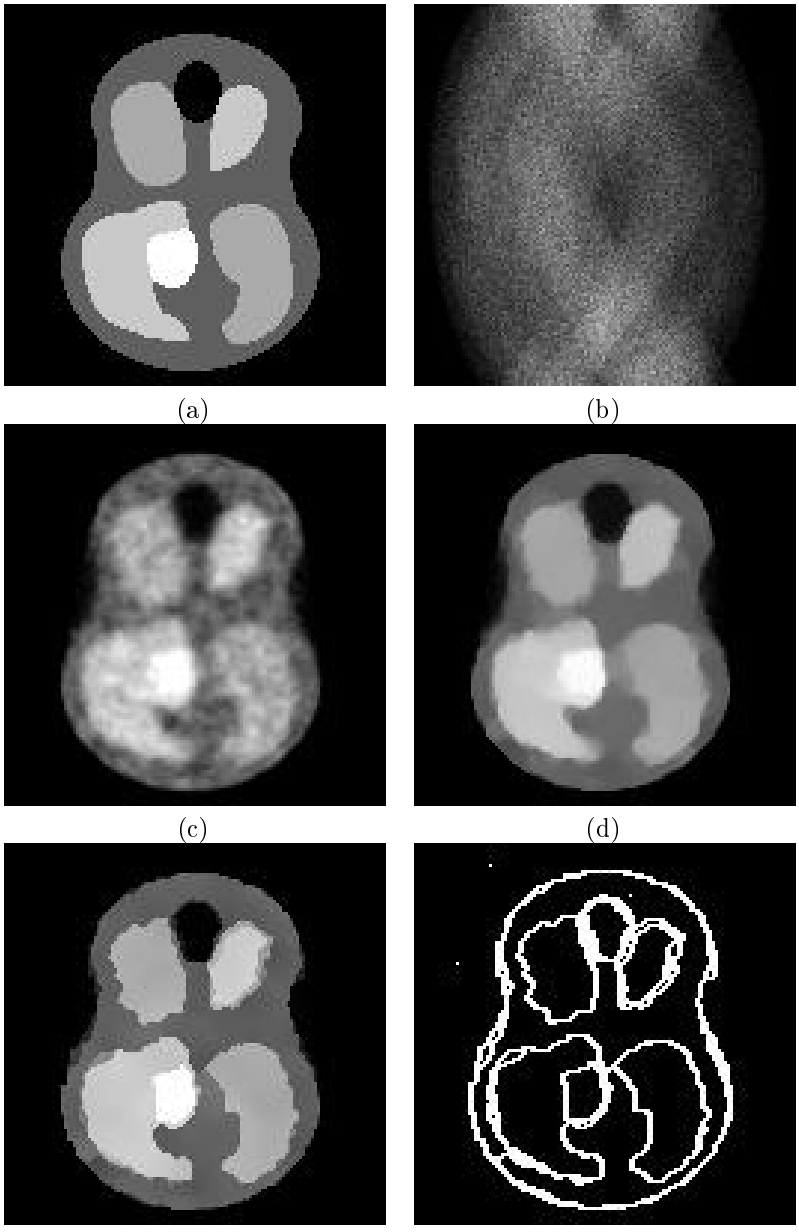

Figure 3: (a) Original image. (b) Simulated sinogram. Reconstruction using a (c) CAR prior, (d) GGMRF prior and (e) CGMRF prior. (f) Line process corresponding to the reconstruction in (e).

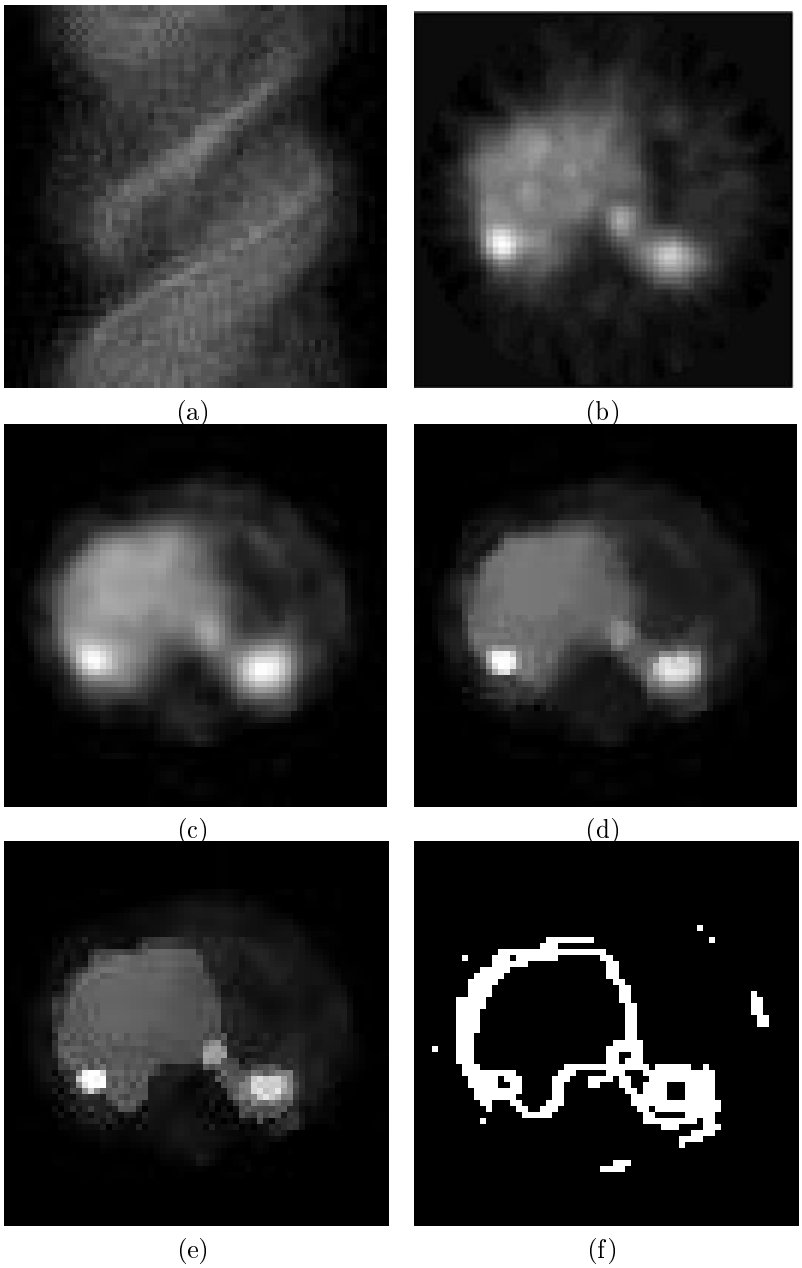

Figure 4: (a) Observed sinogram. Reconstruction using (b) FBP, (c) CAR prior, (d) GGMRF prior and (e) CGMRF prior. (f) Line process corresponding to the reconstruction in (e).

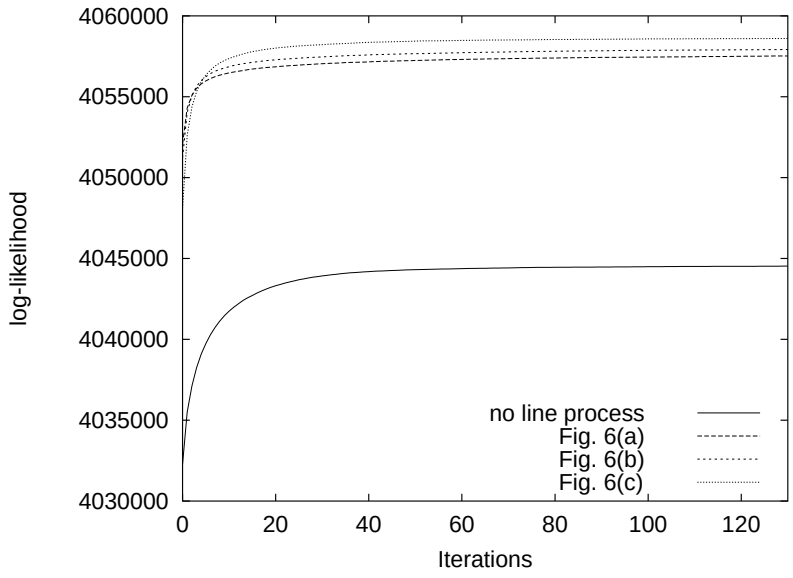

(a)

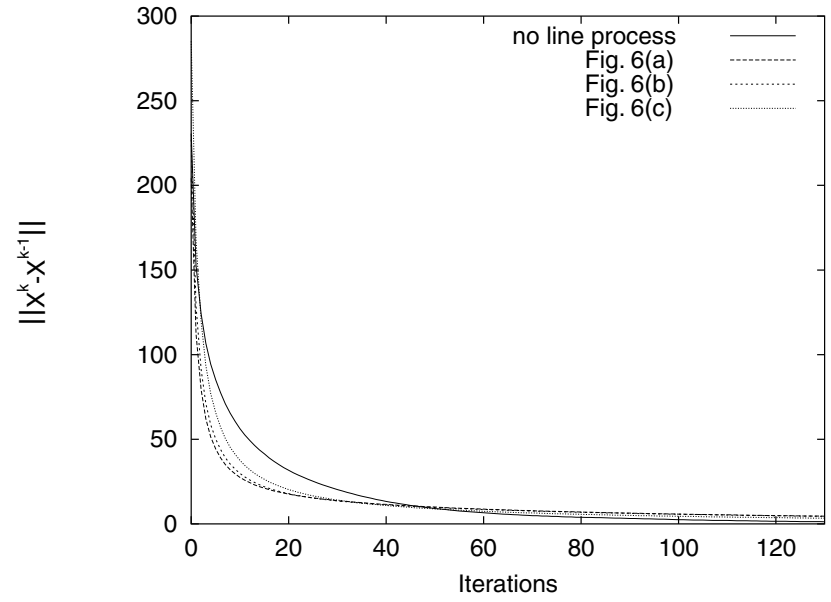

(b)

Figure 5: Convergence results for the synthetic image in Fig. 2(a). (a) Log-likelihood value of the iterative process described in Eq. 10 for the line process configurations shown in Fig. 6, (b) norm of the difference between two consecutive iterations of the iterative process described in Eq. 10 for the line process configurations shown in Fig. 6.

(a) (b) (c)

Figure 6: Fixed line process configurations used in Fig. 5.